The Influence of Cavity Size and Location Within Insulation Paper on the Partial Discharge Activities

Muhammad Hakirin Roslan[1,2], Norhafiz Azis[2,3]*, Mohd Zainal Abidin Ab Kadir[2], Jasronita Jasni[2] and Mohd Fairouz Mohd Yousof[4]

[1]*Faculty of Engineering, Universiti Pertahanan Nasional Malaysia, 57000 UPNM, Kuala Lumpur, Malaysia*
[2]*Advanced Lightning, Power and Energy Research Centre (ALPER), Universiti Putra Malaysia, 43400 UPM, Serdang, Selangor, Malaysia*
[3]*Institute of Nanoscience and Nanotechnology (ION2), Universiti Putra Malaysia, 43400 UPM, Serdang, Selangor, Malaysia*
[4]*Faculty of Electrical and Electronics Engineering, Universiti Tun Hussein Onn Malaysia, 86400 UTHM, Parit Raja, Johor, Malaysia*

ABSTRACT

This paper examines the influence of cavity size and location in the insulation paper on the Partial Discharge (PD) activities through Finite Element Method (FEM). The model consisted of a conductor wrapped with insulation paper. Two different locations of the spherical cavities were introduced in this study, namely Location 1 (L1) and Location 2 (L2), located at the center and left corner of the insulation paper. The model introduced two different sizes of cavities with diameters of 0.5 mm and 0.8 mm. An AC voltage source of 17 kV, 50 Hz, was applied at the conductor while the bottom of the insulation paper was grounded. The real and apparent PDs were obtained by integrating the current flowing through the cavity and ground electrode with the respective surface area. The simulation was carried out for 100 cycles. The resultant model was used to study the PD occurrence, magnitude, and Phase Resolved Partial Discharge (PRPD) within the insulation paper. It is found that the large cavity size produces a lower number of PD occurrences per cycle than the small cavity size. The large cavity size produces a higher charge magnitude as compared with the small cavity size. The PD occurrence per cycle and charge magnitude are higher for the cavity location at L1 compared to L2. The PRPD yields the same pattern for

cavity location at L1 and L2, whereby the differences are only on the charge magnitude and PD occurrence per cycle.

Keywords: Insulation paper, partial discharge modeling, spherical cavity, transformer

INTRODUCTION

One of the parameters that can lead to the possible failure of the transformer is Partial Discharge (PD) (Hussain et al., 2021; Naidu & Kamaraju, 2013; Youssef et al., 2022). PD can exist as a result of either a poor manufacturing process or an insulation aging process. One of the sources of the PD is either the cavity or void in insulations. In recent years, PD monitoring has become one of the crucial methods to evaluate the insulation status. The electrical method is one of the conventional methods to evaluate PD within insulations (IEC60270, 2000; Meitei et al., 2021). PD is a complex phenomenon that produces heat, sound, light, chemical reactions, high-frequency waves, and electrical pulses (CIGRE, 2017; Sikorski et al., 2020; Xavier et al., 2021). Even though PD measurement can provide extensive information on the condition of insulations, PD modeling can further enhance the knowledge of its characteristics.

PD modeling can be classified into capacitance, analytical, and Finite Element Method (FEM) model approaches (Afrouzi et al., 2022). The capacitance model is the first PD model introduced to understand the concept of PD (Whitehead, 1952). An analytical model is also proposed, whereby the surface charge accumulation on the cavity surface due to the previous PD is taken into account, which is not considered in the capacitance model (Pedersen et al., 1995; Pedersen et al., 1991). Nowadays, the reliability of numerical modeling software leads to the introduction of PD modeling based on the FEM model (Borghei, 2022; Forss´en, 2008; Forssén & Edin, 2008; Illias, 2011). This method seems promising due to its ability to model the complex geometry of the electrical equipment. The FEM model has been applied to the cables and wide bandgap power module application for the determination of PD activities (Borghei & Ghassemi, 2019; Borghei & Ghassemi, 2020, 2021; Illias et al., 2016; Joseph et al., 2019).

Both external and internal factors can affect PD activities (Illias et al., 2017). Voltage and frequency are known external factors, while cavity condition, design, and PD mechanism characteristics are classified as internal factors (Borghei et al., 2021; Illias et al., 2011, 2012). The cavity condition mainly involves size and location. Insulation thickness, permittivity, and conductivity, as well as the shape of the conductor, can be included in design characteristics. PD mechanisms include the Electron Generation Rate (EGR) and surface charge accumulation on the cavity surface. Due to the complex winding geometry of the transformer, the effect of the cavity location, as well as cavity size in the insulation paper on the PD activities, needs to be further investigated.

This paper presents the investigation of PD activities within a spherical cavity in the insulation paper of a transformer through FEM modeling. The three-dimensional (3D) model consists of a conductor, insulation paper, and a spherical cavity, solved through an electric transient solver. In this study, the simulation of PD activities is carried out based on the 3D modeling of the active part of the high-voltage winding. It is based on disc-layered high voltage winding of a 33/11 kV, 30 MVA transformer. The Phase Resolved Partial Discharge (PRPD) analysis in the insulation paper with consideration of the spherical cavity location and size is evaluated.

PARTIAL DISCHARGE MECHANISM

Discharge occurs in a defective area, such as a cavity, due to the electron avalanche process, which initiates from the ionization process. Once the electric field in the cavity is sufficient to energize the free electron, it can lead to the multiplication of the number of electrons through collision with neutral atoms. The discharge continues until the electric field in the cavity drops below the extinction field, E_{ext}. The PD inception field, E_{inc} is the minimum electric field to initiate the ionization process. E_{inc} is one of the important mechanisms required to model PD. The second mechanism identifies the number of electrons to initiate the electron avalanche. The final mechanism is the E_{ext}, the minimum electric field required to stop the discharge process.

Partial Discharge Inception Field

The ionization process requires sufficient enhancement of the electric field in the cavity to trigger the movement of the free electron to collide with neutral atoms. The first condition to initiate PD is that the electric field in the cavity must exceed the E_{inc}. In this study, the air-filled cavity was used, which can be calculated based on Equation 1 (Borghei & Ghassemi, 2020; Borghei et al., 2021; Callender & Lewin, 2020).

$$E_{inc} = 24.2P\left(1 + \frac{8.6}{\sqrt{Pd}}\right) \qquad unit\ in\ \frac{V}{m} \qquad\qquad [1]$$

P and d in Equation 1 referred to the cavity pressure and diameter, which were set to 100 kPa, and 2 different sizes of the cavities with a diameter of 0.5 mm and 0.8 mm.

Partial Discharge Extinction Field

E_{ext} was determined based on Equation 2, where the value was set to 10% of E_{inc} value calculated from Equation 1 (Joseph et al., 2019).

$$E_{ext} = 0.1E_{inc} \qquad\qquad unit\ in\ \frac{V}{m} \qquad\qquad [2]$$

Electron Generation Rate

Apart from the electric field in the cavity needing to exceed the E_{inc}, the availability of the free electron is also required to initiate the ionization process. The lack of the free electron causes the PD occurrence to be delayed even if the first condition, the E_{inc}, is satisfied. The time delay refers to the statistical time lag, τ_{stat}, related to the electron generation. The sources of electron generation are volume ionization and surface emission.

(i) Volume ionization

Electron generation from the volume ionization is normally due to the gas ionization by irradiation of photons (Borghei et al., 2021). In this study, the electron generation from volume ionization was set as a constant value throughout the simulation, denoted by N_{vol} (Illias, 2011; Pan et al., 2019).

(ii) Surface emission

Electron Generation Rate (EGR) from surface emission was not considered for the first discharge of PD due to the unavailability of charge accumulation at the surface of the cavity. After the first PD occurrence, the charge from the previous PD accumulates at the surface of the cavity. The effect of the surface charge decay was considered in calculating EGR from the surface emission. In this study, the EGR from surface emission was set as time-dependent, denoted by $N_{surf}(t)$, whereby the number of electrons changed with time.

This study calculated the total EGR denoted by $N_{tot}(t)$ based on Equation 3 (Illias, 2011; Pan et al., 2019).

$$N_{tot}(t) = N_{surf}(t) + N_{vol} \qquad , \qquad unit\ in\ \frac{1}{s} \qquad [3]$$

Where N_{vol} is a constant value that was set to 1 s^{-1}, and $N_{surf}(t)$ is a time-dependent value that can be calculated based on Equation 4 (Illias, 2011).

$$N_{surf}(t) = N_{PD}\exp\left(\frac{E_{cav}(t)}{E_{inc}}\right)\exp\left(\frac{-(t-t_{PD})}{t_{decay}}\right) \quad , \qquad unit\ in\ \frac{1}{s} \qquad [4]$$

Where the influence of the electric field on surface emission was represented in the first term of the exponential function, the second exponential function represented the effect of surface charge decay deposited by the previous PD. Based on the previous study, the t_{decay} was set to 2 ms at ambient temperature conditions (Illias et al., 2012). N_{PD} is the number of electrons available due to previous PD, which can be calculated by Equation 5 (Illias, 2011).

$$N_{PD} = N_{s0}\frac{E_{cav}(t_{PD})}{E_{inc}} \qquad , \qquad unit\ in\ \frac{1}{s} \qquad [5]$$

Where N_{s0} is the initial electron available, and its value depends on the polarity of the electric field previous PD, $E_{cav}(PD1)$, and the next PD occurrence, $E_{cav}(PD2)$, as shown in Equation 6 (Illias, 2011). The N_{s0} is high when no polarity changes exist between $E_{cav}(PD1)$ and $E_{cav}(PD2)$. Otherwise, the N_{s0} is low due to the assumption of the effect of surface charge decay. As a result, it can lead to a high statistical time lag.

$$N_{s0} = \begin{cases} N_{s0Low} & when \ \dfrac{E_{cav}(PD2)}{E_{cav}(PD1)} < 0 \\[2mm] N_{s0Higher} & when \ \dfrac{E_{cav}(PD2)}{E_{cav}(PD1)} > 0 \end{cases} \qquad [6]$$

The values of N_{s0Low} and $N_{s0Higher}$ depend on the cavity size, whereby based on the previous study, the values for large cavity size are lower than for small cavity size (Illias et al., 2012).

FINITE ELEMENT METHOD MODEL

Electric field distribution computation in the dielectric is important in PD modeling. Therefore, the FEM was employed to compute the electric field distribution. In this study, FEM based on Ansys Maxwell was utilized to compute the electric field distribution in the insulation paper as well as a spherical cavity. The electric transient solver was used in this study to solve for the electric potential as well as the electric field distribution.

Phase Resolved Partial Discharge Simulation

The discharge process used in this study was the conductance method. The discharge process was modeled through increments of the cavity conductivity from the initial state to a high value. Figure 1 shows the flowchart of the PD process algorithm. The process started with the initialization of the modeling parameters in the simulation, as shown in Table 2. The simulation was carried out at each time step during no PD. At each of the time steps, the electric field in the cavity was extracted and compared with the inception field to evaluate the first condition of the PD occurrence. The time step was increased until the electric field in the cavity exceeded the inception field, and the process continued to evaluate the second condition of PD occurrence, which was the availability of the free electron. Once both conditions were satisfied, the total EGR was calculated, and the probability of PD occurrence was determined based on Equation 7 (Forssén & Edin, 2008; Illias, 2011; Pan et al., 2019). Since the PD occurrence was stochastic, the probability was compared with the random number, R, ranging from 0 to 1. If the probability was higher than the R, the discharge process was modeled, increasing the cavity conductivity. Due to the increment of the cavity conductivity, the electric field in the cavity decreased until the electric field

in the cavity was less than the E_{ext}, whereby the cavity conductivity was reset to the initial value. The apparent and real charges were determined based on the current integration flowing through the ground electrode and cavity center surface area. Once the simulation step reached 100 cycles, the simulation stopped, and PRPD was plotted.

$$P(t) = N_{tot}(t)\Delta t \qquad\qquad [7]$$
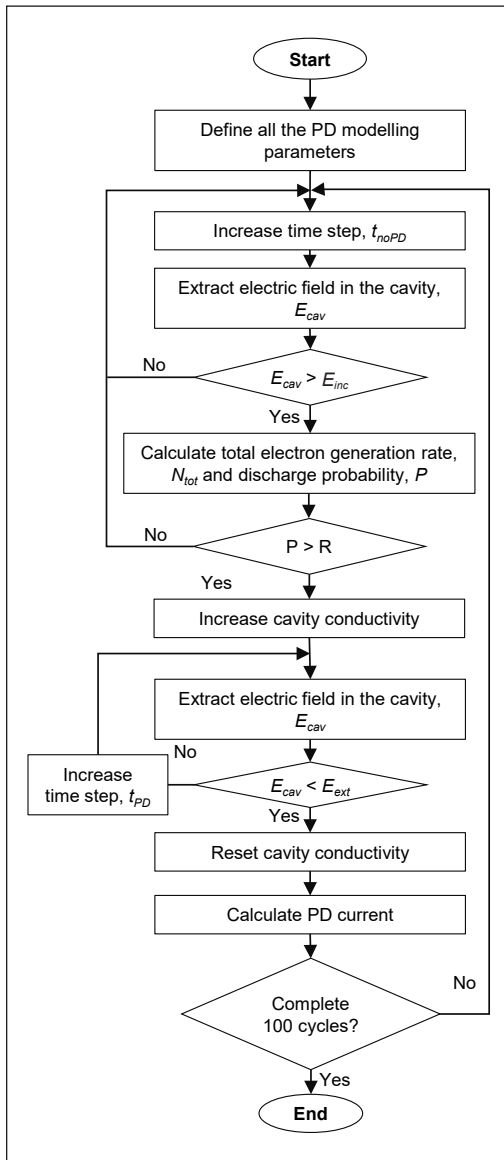
Figure 1. Flowchart of the phase-resolved partial discharge simulation

Model Geometry and Partial Discharge Model Parameters

The 3D model geometry consists of insulation paper and a conductor, as shown in Figure 2. The model was developed in Ansys Maxwell using an electric transient solver to solve the electric potential distribution in the 3D model. It was modeled based on the active part of the disc-layered high voltage winding in a 33/11 kV, 30 MVA transformer.

The spherical cavity was introduced within the insulation paper to represent the defect area. The details of the geometrical design can be seen in Table 1 (Murthy et al., 2020). The details of the PD modeling parameters for the simulation are shown in Table 2. The relative permittivity of the insulation paper, ε_{mat}, used in this study was 2.3, according to (Murthy et al., 2020). The
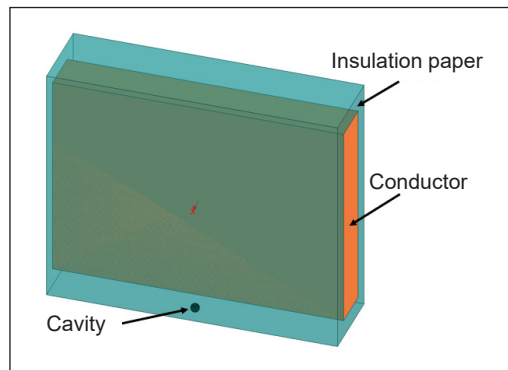

Figure 2. 3D model geometry of insulation paper and conductor

Table 1
Parameter for 3D finite element method model

| Parameters	Values
Height (conductor)	11.5 mm
Width (conductor)	2.4 mm
Length (conductor)	16 mm
The thickness of the insulation paper	1 mm
Cavity diameter	0.5 mm and 0.8 mm
Total mesh elements	255932

Table 2
Parameter for partial discharge modeling of the insulation paper and cavity

Parameters	Values	Units
Insulation paper (relative permittivity), ε_{mat}	2.3	
Cavity (relative permittivity), ε_{cav}	1	
Insulation paper (conductivity), σ_{mat}	1×10^{-10}	s/m
Conductivity of cavity during no PD, $\sigma_{cav,0}$	0	s/m
Conductivity of cavity during PD, $\sigma_{cav,PD}$	5×10^{-3}	s/m
Simulation time step (no PD), t_{noPD}	100	μs
Simulation time step during PD, t_{PD}	1	ns

relative permittivity of the spherical cavity, ε_{cav}, was set to 1 since the cavity was assumed to contain only air. The conductivities of insulation paper, σ_{mat}, are reported between 0.05×10^{-12} and 1.2×10^{-12} s/m (Saha & Purkait, 2008; Xiao et al., 2013). However, the electric field distribution in insulation paper is less affected by σ_{mat} if the value is too small based on simulation using the FEM (Illias, 2011). Therefore, the conductivity was set to 1×10^{-10} s/m in the simulation. The conductivity of the cavity during no PD, $\sigma_{cav,0}$ was 0 s/m since there is no current flowing in the cavity. During the PD occurrence, the conductivity of the cavity, $\sigma_{cav,PD}$ was set to 5×10^{-3} s/m, according to Illias (2011). This value is found suitable to avoid the fast reduction of the electric field as well as reduce the simulation time. The time step during no PD was set to 100 μs, which is suitable to avoid long simulation time. The time step during PD was set to 1 ns since the PD could be initiated in the range between micro and nanoseconds (CIGRE, 2017; Morsalin & Das, 2020). An AC voltage source of 17 kV, 50 Hz AC was supplied at the conductor since it is high enough to exceed the PD inception field in this study. The bottom of the insulation paper was grounded.

In this study, 2 different locations of the spherical cavities were introduced, namely Location 1 (L1) and Location 2 (L2), located at the center and left corner of the insulation papers. In addition, 2 different sizes of cavities with a diameter of 0.5 mm and 0.8 mm were introduced in the model, as shown in Figure 3.
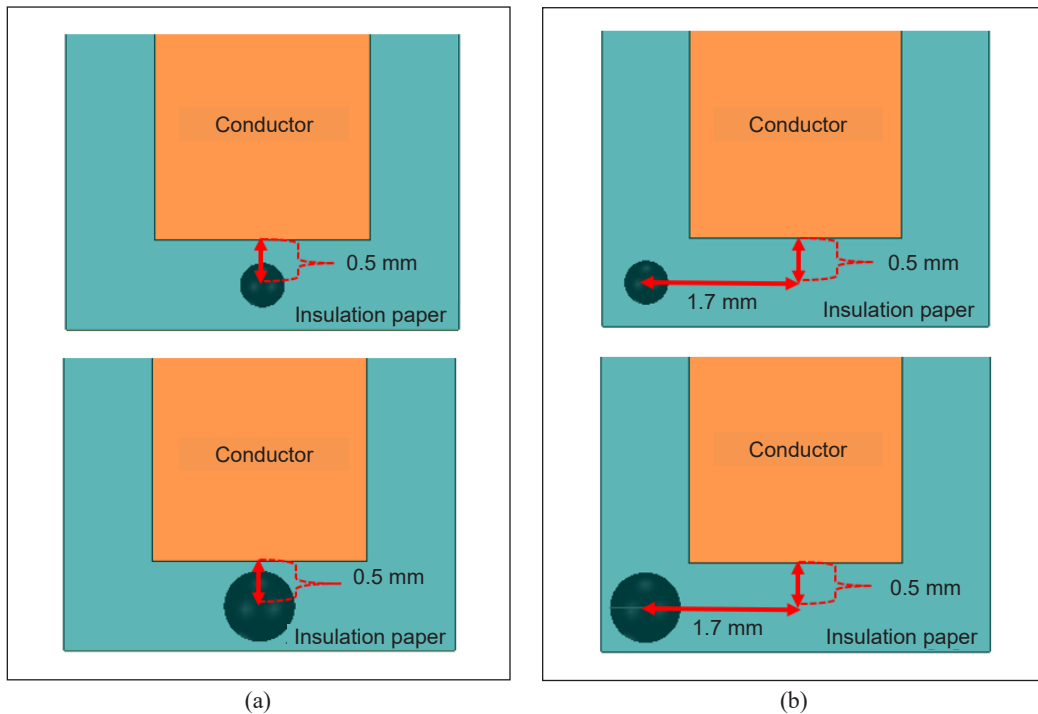
Figure 3. Two different cavity sizes and locations within the insulation paper: (a) Side view (L1); and (b) Side view (L2)

RESULTS

Phase Resolved Partial Discharge Pattern for the 0.5 mm Cavity Size in the Insulation Paper

The real charge magnitude PRPD pattern in the insulation paper for the cavity with a diameter of 0.5 mm at L1 is shown in Figure 4. The PD occurrence is mostly generated at the E_{inc} or minimum charge magnitude with the highest repetition rate. The highest charge magnitude is generated at the phases from 60° to 90° as well as from 240° to 270°. A similar PRPD pattern is recorded for the apparent charge magnitude, as shown in Figure 5. However, the charge magnitude is lower than the real charge magnitude. It is expected due to the apparent charge magnitude is the induced charge calculated at the ground electrode.

The PRPD pattern of real charge magnitude in the insulation paper for the cavity with a diameter of 0.5 mm at L2 is shown in Figure 6. Most of the PD occurrences are recorded at E_{inc} or at the minimum level charge magnitude with the highest number of repetition rates at the phases from 45° to 90° as well as from 210° to 270°. The highest charge magnitude is generated at the phases from 60° to 90° as well as from 240° to 270°. Figure 7 shows the PRPD pattern of apparent charge magnitude whereby the pattern is similar to the real charge PRPD with the difference only in charge magnitude.
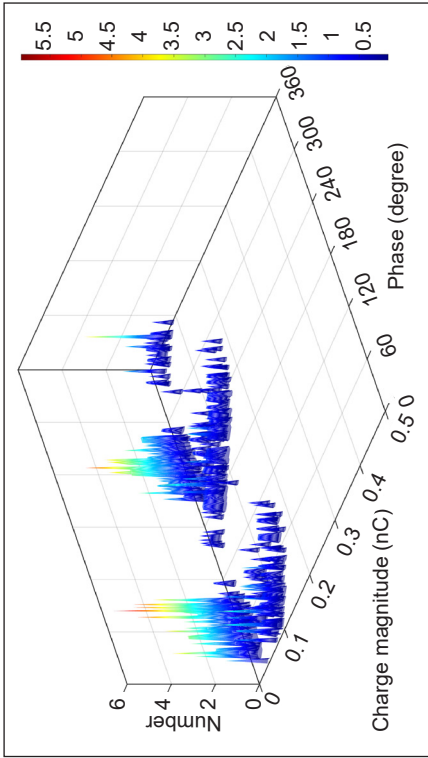
Figure 5. The phased resolved partial discharge pattern of apparent charge magnitude in the insulation paper for the cavity diameter of 0.5 mm at L1
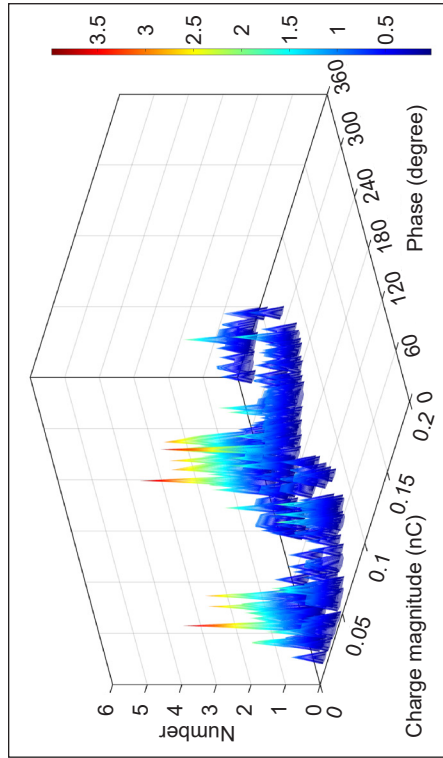
Figure 7. The phase resolved a partial discharge pattern of apparent charge magnitude in the insulation paper for the cavity with a diameter of 0.5 mm at L2
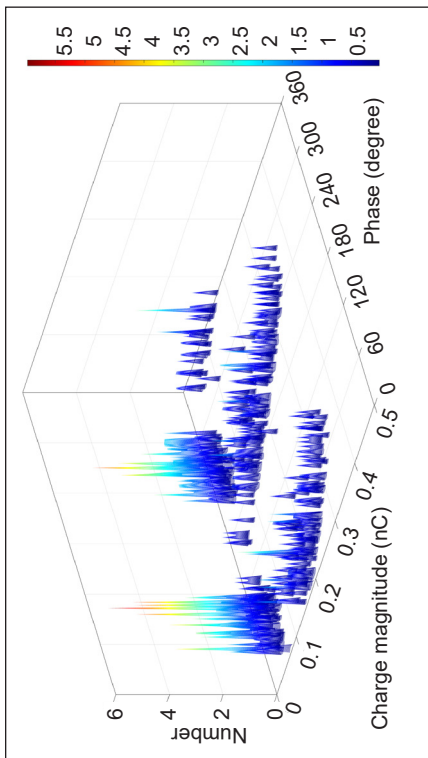
Figure 4. The phase-resolved partial discharge pattern of real charge magnitude in the insulation paper for the cavity diameter of 0.5 mm at L1
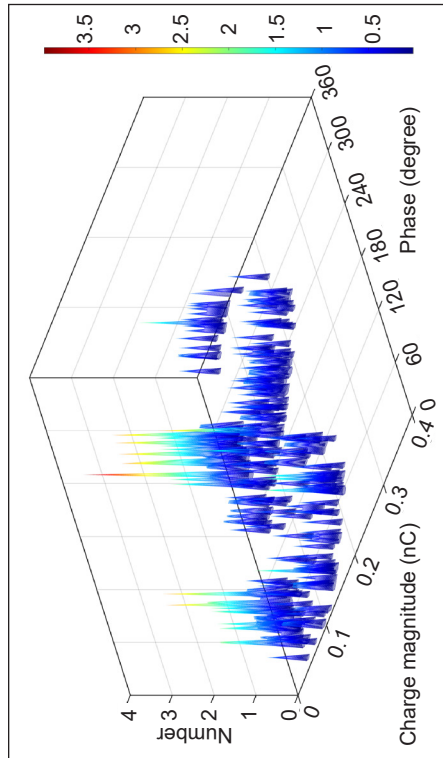
Figure 6. The phase-resolved partial discharge pattern of real charge magnitude in the insulation paper for the cavity diameter of 0.5 mm at L2

Phased Resolved Partial Discharge Pattern for the 0.8 mm Cavity Size in the Insulation Paper

The PRPD pattern of real and apparent charge magnitudes in the insulation paper for the cavity with a diameter of 0.8 mm at both locations at L1 and L2 are shown in Figures 8, 9, 10, and 11. In terms of cavity location at L1, the PRPD pattern for both real and apparent charge magnitudes are similar, but the differences are only in the amplitude, as shown in Figures 8 and 9. The charge magnitude is highest at the phases from 60° to 120° as well as from 240° and 300°. The charge distribution is evenly distributed over the phase range. The PD repetition rate at each phase and charge magnitude ranges are close to each other, with the repetition rate ranging from 0.5 to 2.

A similar PRPD pattern as L1 is recorded in the insulation paper for the cavity with a diameter of 0.8 mm at L2, as shown in Figures 10 and 11. However, the charge magnitude is slightly lower as compared with L1. The PD occurrence at L1 is also higher than at L2 based on the PRPD pattern intensity, as shown in Figures 8, 9, 10, and 11.

Partial Discharge Activities for Different Cavity Sizes and Locations

The PD parameters in the insulation paper for different cavity sizes and locations with consideration of τ_{stat} are shown in Table 3. The PD occurrence per cycle is 5.12 cycles for both real and apparent charge magnitudes at L1 for the cavity with a diameter of 0.5 mm. However, the PD occurrence per cycle at L2 for the same cavity size is lower than L1 with 3.04 cycles. The PD occurrence per cycle is slightly low for the cavity with a diameter of 0.8 mm at both locations, which are 3.05 cycles at L1 and 2.17 cycles at L2.

The charge magnitude in terms of maximum, minimum, and mean charges for the cavity with a diameter of 0.5 mm are lower than the cavity with a diameter of 0.8 mm, as shown in Table 3. The charge magnitude is higher for the cavity location at L1 as compared with L2, regardless of the cavity size.

Table 4 shows the PD parameters in the insulation paper for different cavity sizes and locations without consideration of τ_{stat}. The PD occurrence per cycle is higher for the cavity

Table 3

Partial discharge parameters in the insulation paper for different cavity sizes and locations considering τ_{stat}

Parameters	Cavity Location at L1				Cavity location at L2			
Cavity size	0.5 mm		0.8 mm		0.5 mm		0.8 mm	
	Real	Apparent	Real	Apparent	Real	Apparent	Real	Apparent
PD occurrence per cycle	5.12	5.12	3.05	3.05	3.04	3.04	2.17	2.17
Total charge per cycle, pC	684	342	1806	1295	341	124	821	479
Mean Charge, pC	134	67	592	424	112	41	378	221
Maximum charge, pC	368	184	1179	845	240	87	688	402
Minimum charge, pC	50	25	145	104	44	16	113	66
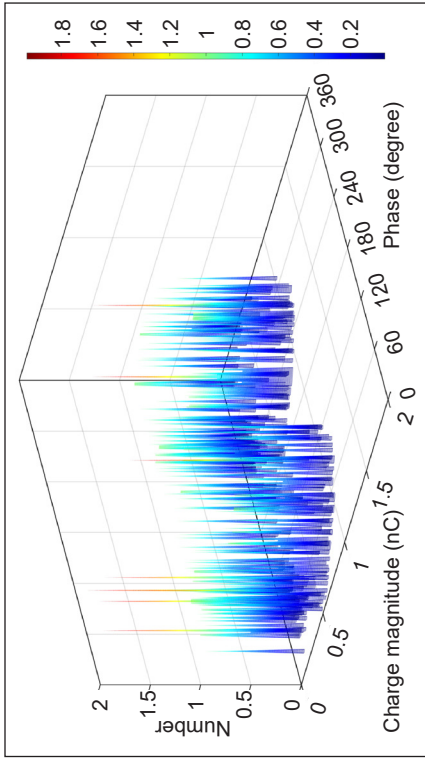
Figure 9. The phase resolved a partial discharge pattern of apparent charge magnitude in the insulation paper for the cavity with a diameter of 0.8 mm at L1

Figure 8. The phase-resolved partial discharge pattern of real charge magnitude in the insulation paper for the cavity with a diameter of 0.8 mm at L1
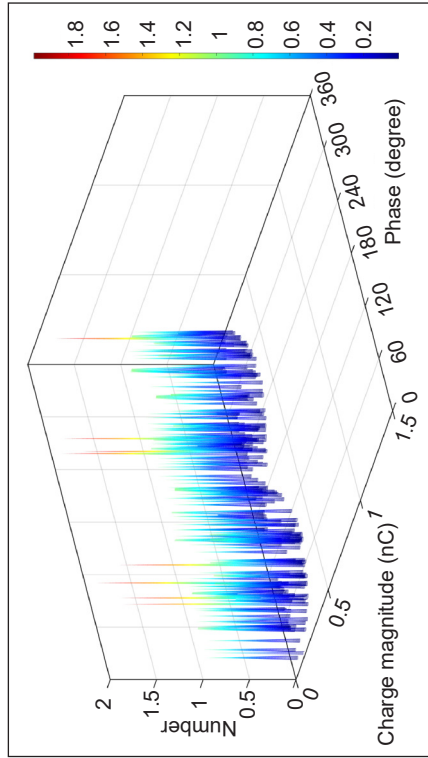
Figure 11. The phased resolved partial discharge pattern of apparent charge magnitude in the insulation paper for the cavity with a diameter of 0.8 mm at L2
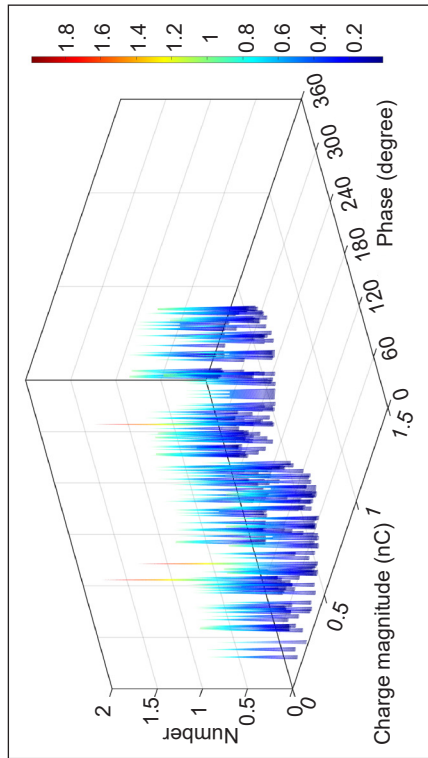
Figure 10. The phase resolved the partial discharge pattern of real charge magnitude in the insulation paper for the cavity with a diameter of 0.8 mm at L2

Table 4

Partial discharge parameters in the insulation paper for different cavity sizes and locations without consideration of τ_{stat}

Parameters	Cavity Location at L1				Cavity location at L2			
Cavity size	0.5 mm		0.8 mm		0.5 mm		0.8 mm	
	Real	Apparent	Real	Apparent	Real	Apparent	Real	Apparent
PD occurrence per cycle	11.99	11.99	16.00	16.00	7.99	7.99	11.99	11.99
Total charge per cycle, pC	600	300	2320	1664	352	128	1355	791
Mean Charge, pC	50	25	145	104	44	16	113	66
Maximum charge, pC	50	25	145	104	44	16	113	66
Minimum charge, pC	50	25	145	104	44	16	113	66

location at L1 as compared with L2. A similar finding is observed with consideration of τ_{stat} (Table 3). In terms of cavity size, the PD occurrence per cycle is higher for the large cavity size as compared with the small size. However, this condition is the opposite when the τ_{stat} is considered, whereby the large cavity size produces lower PD occurrence per cycle as compared with a smaller cavity. The maximum, minimum, and mean charge values without consideration of τ_{stat} are the same for each of the conditions due to the PD occurrence only at the inception field level at 5.4 kV/mm and 4.75 kV/mm for cavities with diameters of 0.5 mm and 0.8 mm, respectively (Table 4).

DISCUSSION

Based on the result in Table 3, the PD occurrence per cycle is higher in the insulation for the cavity location at L1 than in L2, regardless of the cavity size. A similar pattern is found for the charge magnitude whereby the cavity at L1 produces a higher charge magnitude than L2. It is due to the electric field in the cavity is higher at L1 as compared with L2. Figure 12 shows the electric field in the cavity, whereby it is simulated for 1 cycle based on the condition in the absence of PD activity. The electric field in the cavity is higher at L1 than at L2. The sharp edge of the conductor and the location of the cavity within the insulation paper can affect the electric field distribution in the insulation paper even if the same electric potential is injected at the conductor, whereby the electric field at L1 is slightly higher than at L2, as shown in Figure 13. The time to reach the E_{inc} is faster at L1 (t_{L1}) than at L2 (t_{L2}), which leads to the increment of the PD occurrence per cycle as well as charge magnitude.

In terms of cavity size, the large cavity size produces a lower PD occurrence per cycle as compared with the small cavity size because the large cavity size can cause a high charge decay rate due to the high free charges accumulated on the cavity surface, which increases the cavity surface conduction. This condition reduces the number of free electrons as well as the EGR. However, the large cavity size generates a higher charge magnitude as
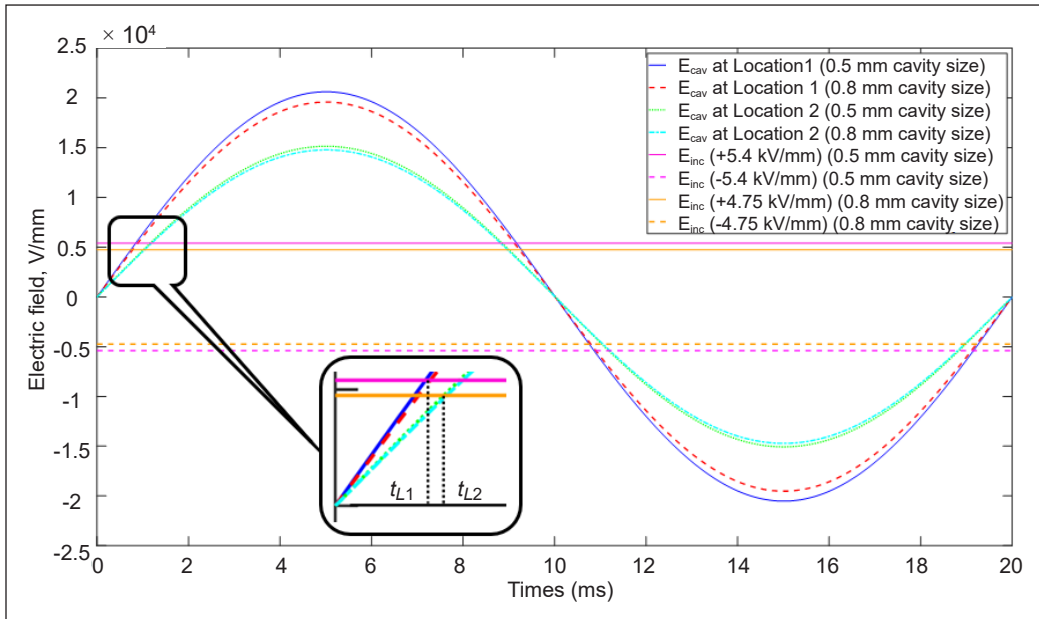
Figure 12. Electric field in the cavity versus time for one cycle in the absence of partial discharge activity
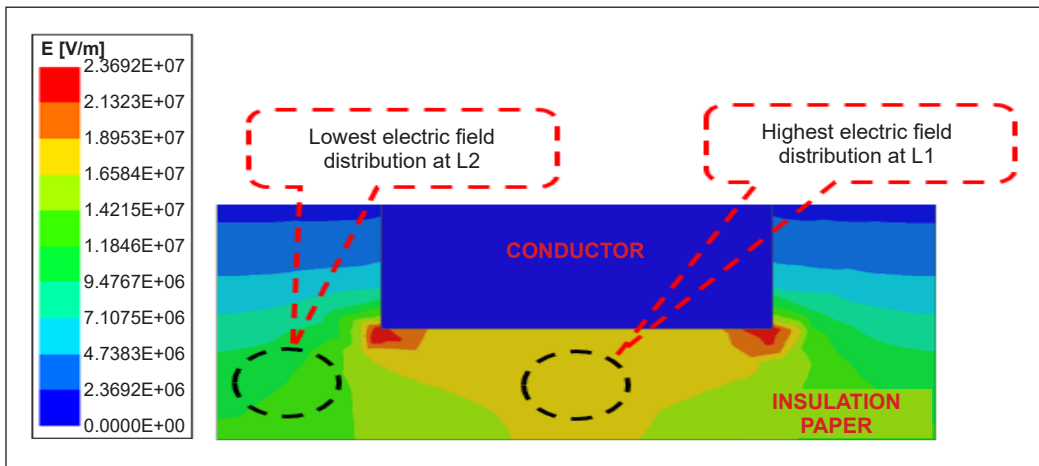

Figure 13. Electric field distribution in the insulation paper in the absence of partial discharge activity

compared with a small cavity. The large cavity size increases the length of the avalanche propagation, leading to high charge magnitude.

CONCLUSION

PD modeling based on FEM can be used to examine the PD activity in terms of the PRPD pattern within a spherical cavity in the insulation paper. The PRPD pattern for a cavity with a diameter of 0.5 mm produces the same pattern for both locations, L1 and L2, whereby the

PD is distributed mostly at the minimum charge magnitude or PD occurrence at the E_{inc}. However, the charge magnitude, as well as PD occurrence, is higher at L1 as compared with L2. The PRPD pattern for the cavity with a diameter of 0.8 mm yields the same pattern for both locations, L1 and L2. However, the pattern differs from a cavity with a diameter of 0.5 mm, whereby the PD occurrence is distributed at all phase ranges and produces lower PD occurrence per cycle. On the other hand, the charge magnitude for the cavity with a diameter of 0.8 mm is higher as compared with the cavity with a diameter of 0.5 mm. In conclusion, the cavity location at L1 produces higher charge magnitude and PD occurrence per cycle as compared with L2. In addition, the large cavity size produces a higher charge magnitude but fewer PD occurrences per cycle than a small cavity.

ACKNOWLEDGMENT

REFERENCES

Afrouzi, H. N., Hassan, A., Chee, D. T. Y., Mehranzamir, K., Malek, Z. A., Mashak, S. V., & Ahmed, J. (2022). In-depth exploration of partial discharge modelling methods within insulations. *Cleaner Engineering and Technology, 6*, Article 100390. https://doi.org/10.1016/j.clet.2021.100390

Borghei, M., & Ghassemi, M. (2019). Partial discharge analysis under high-frequency, fast-rise square wave voltages in silicone gel: A modeling approach. *Energies, 12*(23), Article 4543. https://doi.org/10.3390/en12234543

Borghei, M., & Ghassemi, M. (2020). A finite element analysis model for partial discharges in silicone gel under a high slew rate, high-frequency square wave voltage in low-pressure conditions. *Energies, 13*(9), Article 2152. https://doi.org/10.3390/en13092152

Borghei, M., & Ghassemi, M. (2021). Characterization of partial discharge activities in WBG power converters under low-pressure condition. *Energies, 14*(17), Article 5394. https://doi.org/10.3390/en14175394

Borghei, M., Ghassemi, M., Rodriguez-Serna, J. M., & Albarracin-Sanchez, R. (2021). A finite element analysis and an improved induced charge concept for partial discharge modeling. *IEEE Transactions on Power Delivery, 36*(4), 2570-2581. https://doi.org/10.1109/tpwrd.2020.2991589

Borghei, S. M. R. (2022). *Partial discharges: Experimental investigation, model development, and data analytics* [Doctoral dissertation]. Virgina Polytechnic Institue, USA. http://hdl.handle.net/10919/108321

Callender, G., & Lewin, P. L. (2020). Modeling Partial Discharge Phenomena. *IEEE Electrical Insulation Magazine*, *36*(2), 29-36.

CIGRE. (2017). *Partial discharges in transformers* (Working Group D1.29). CIGRE. https://www.slideshare.net/PowerSystemOperation/partial-discharges-in-transformers

Forssén, C. (2008). *Modelling of cavity partial discharges at variable applied frequency* [Doctoral dissertation]. KTH, Sweden. https://www.diva-portal.org/smash/record.jsf?pid=diva2%3A13791&dswid=6945

Forssén, C., & Edin, H. (2008). Partial discharges in a cavity at variable applied frequency Part 2: Measurements and modeling. *IEEE Transactions on Dielectrics and Electrical Insulation, 15*(6), 1610-1616. https://doi.org/10.1109/TDEI.2008.4712664

Hussain, M. R., Refaat, S. S., & Abu-Rub, H. (2021). Overview and partial discharge analysis of power transformers: A literature review. *IEEE Access, 9*, 64587-64605. https://doi.org/10.1109/access.2021.3075288

IEC60270. (2000). *High-voltage test techniques - Partial discharge measurements.* British Standard. http://teslapishro.ir/wp-content/uploads/2019/12/High-voltage-test-technique.pdf

Illias, H. A. (2011). *Measurement and simulation of partial discharges within a spherical cavity in a solid dielectric material* [Doctoral dissertation] University of Southampton, UK. https://eprints.soton.ac.uk/194921/1/HazleeThesis_EPRINTS.pdf

Illias, H. A., Chen, G., & Lewin, P. L. (2011). Partial discharge behavior within a spherical cavity in a solid dielectric material as a function of frequency and amplitude of the applied voltage. *IEEE Transactions on Dielectrics and Electrical Insulation, 18*(2), 432-443. https://doi.org/10.1109/tdei.2011.5739447

Illias, H. A., Chen, G., & Lewin, P. L. (2012). Partial discharge within a spherical cavity in a dielectric material as a function of cavity size and material temperature. *IET Science, Measurement & Technology, 6*(2), 52-62. https://doi.org/10.1049/iet-smt.2011.0091

Illias, H. A., Chen, G., & Lewin, P. L. (2017). Comparison between three-capacitance, analytical-based and finite element analysis partial discharge models in condition monitoring. *IEEE Transactions on Dielectrics and Electrical Insulation, 24*(1), 99-109. https://doi.org/10.1109/tdei.2016.005971

Illias, H. A., Tunio, M. A., Bakar, A. H. A., Mokhlis, H., & Chen, G. (2016). Partial discharge phenomena within an artificial void in cable insulation geometry: Experimental validation and simulation. *IEEE Transactions on Dielectrics and Electrical Insulation, 23*(1), 451-459. https://doi.org/10.1109/tdei.2015.005155

Joseph, J., Mohan, S., & Thiruthi Krishnan, S. (2019). Numerical modelling, simulation and experimental validation of partial discharge in cross-linked polyethylene cables. *IET Science, Measurement & Technology, 13*(2), 309-317. https://doi.org/10.1049/iet-smt.2018.5248

Meitei, S. N., Borah, K., & Chatterjee, S. (2021). Partial discharge detection in an oil-filled power transformer using fiber bragg grating sensors: A review. *IEEE Sensors Journal, 21*(9), 10304-10316. https://doi.org/10.1109/jsen.2021.3059931

Morsalin, S., & Das, N. (2020). Diagnostic aspects of partial discharge measurement at very low frequency: A review. *IET Science, Measurement & Technology, 14*(10), 825-841. https://doi.org/10.1049/iet-smt.2020.0225

Murthy, A. S., Azis, N., Jasni, J., Othman, M. L., Mohd Yousof, M. F., & Talib, M. A. (2020). Extraction of winding parameters for 33/11 kV, 30 MVA transformer based on finite element method for frequency response modelling. *PLoS One, 15*(8), Article e0236409. https://doi.org/10.1371/journal.pone.0236409

Naidu, M. S., & Kamaraju, V. (2013). *High Voltage Engineering*. McGraw Hill.

Pan, C., Chen, G., Tang, J., & Wu, K. (2019). Numerical modeling of partial discharges in a solid dielectric-bounded cavity: A review. *IEEE Transactions on Dielectrics and Electrical Insulation, 26*(3), 981-1000. https://doi.org/10.1109/tdei.2019.007945

Pedersen, A., Crichton, G. C., & McAIIister, I. W. (1995). The functional relation between partial discharges and induced charge. *IEEE Transactions on Dielectrics and Electrical Insulation, 2*(4), 535-543. https://doi.org/10.1109/94.407019

Pedersen, A., Crichton, G. C., & McAlIister, I. W. (1991). The theory and measurement of partial discharge transients. *IEEE Transactions on Electrical Insulation, 26*(3), 487-497. https://doi.org/10.1109/14.85121

Saha, T. K., & Purkait, P. (2008). Understanding the impacts of moisture and thermal ageing on transformer's insulation by dielectric response and molecular weight measurements. *IEEE Transactions on Dielectrics and Electrical Insulation, 15*(2), 568-582. https://doi.org/10.1109/TDEI.2008.4483479

Sikorski, W., Walczak, K., Gil, W., & Szymczak, C. (2020). On-line partial discharge monitoring system for power transformers based on the simultaneous detection of high frequency, ultra-high frequency, and acoustic emission signals. *Energies, 13*(12), Article 3271. https://doi.org/10.3390/en13123271

Whitehead, S. (1952). Electrical breakdown of solids. *Nature, 170*(4319), Article 219. https://doi.org/10.1038/170219a0

Xavier, G. V. R., Silva, H. S., da Costa, E. G., Serres, A. J. R., Carvalho, N. B., & Oliveira, A. S. R. (2021). Detection, classification and location of sources of partial discharges using the radiometric method: Trends, challenges and open issues. *IEEE Access, 9*, Article 110787-110810. https://doi.org/10.1109/access.2021.3102888

Xiao, L., Ruijin, L., Maochang, L., Lijun, Y., Junkun, Y., & Chaoliang, Q. (2013, October 20-23). *Influence of aging degree on polarization and depolarization currents of oil-paper insulation* [Paper presentation]. Annual Report Conference on Electrical Insulation and Dielectric Phenomena, Chenzhen, China. https://doi.org/10.1109/CEIDP.2013.6748255

Youssef, M. M., Ibrahim, R. A., Desouki, H., & Moustafa, M. M. Z. (2022, March 4-6). *An Overview on Condition Monitoring & Health Assessment Techniques for Distribution Transformers* [Paper presentation]. 6th International Conference on Green Energy and Applications (ICGEA), Singapore. https://doi.org/10.1109/ICGEA54406.2022.9791900